WILEY-VCH

DOI: 10.1002/ ((please add manuscript number))
Article type: Full Paper

Low energetic loss DPP donor and non-fullerene acceptor organic solar cells with high quantum efficiencies

Xin Song, Nicola Gasparini, Masrur Morshed Nahid, Sri Harish Kumar Paleti, Cheng Li, Weiwei Li, Harald Ade, Derya Baran*

X. Song, S. H. K. Paleti, Dr. N. Gasparini, Prof. D. Baran
King Abdullah University of Science and Technology (KAUST), Division of Physical Sciences and Engineering (PSE), KAUST Solar Center (KSC), Thuwal, Saudi Arabia.

Dr. M. M. Nahid, Prof. H. Ade
Department of Physics, Organic and Carbon Electronics Lab (ORaCEL), North Carolina State University, Raleigh, NC 27695, USA

Dr. C. Li, Prof. W. Li
State Key Laboratory of Organic-Inorganic Composites, Beijing University of Chemical Technology, Beijing 100029, P. R. China

Corresponding author email: derya.baran@kaust.edu.sa

Abstract: Diketopyrrolopyrrole (DPP)-based polymers have gained a significant research interest in the organic electronics community because of their high charge carrier mobilities in organic field-effect transistors (OFETs) and their ability to harvest near-infrared (NIR) photons in organic solar cells (OSCs). However, DPP-based devices still face the challenge of the trade-off between energetic loss (E_{loss}) and maximum external quantum efficiency (EQE_{max}). Herein, by combining a low-lying ionization potential DPP polymer (PBDTT-DPP) and IEICO-4F as electron-acceptor, we obtain a power conversion efficiency (PCE) of 8.14%. Due to the low E_{loss} (0.57 eV) along with high EQE_{max} (>70%), PBDTT-DPP:IEICO-4F devices deliver high J_{sc} of 18.5 mA cm^{-2} without sacrificing V_{oc} (0.68 V). An in-depth investigation, comprising of optoelectronic and nanostructural characterizations of PBDTT-DPP with different non fullerene acceptors (NFAs), suggests that better texture and molecular packing in the IEICO-4F blends improve charge transport and reduce charge recombination. Additionally, we demonstrate a champion efficiency of 9.68% by engineering hole-transporting and electron-transporting layers, Our work indicates the great potential of high efficiency OSCs based on DPP polymer donor:NFA and provide an important guideline for further NFA molecular optimization for DPP-based solar cells.

1. Introduction

Over the past few decades, bulk heterojunction (BHJ) organic solar cells (OSCs) have attracted great interest because of their unique properties, such as semi-transparency and solution-processability for large-scale fabrication.[1–4] For many years, OSC research and progress have been dominated by active layers comprised of blend of a fullerene derivate ([6,6]-phenyl-C_{61} butyric acid methyl ester ($PC_{61}BM$) and its C_{71} analogue) as the electron acceptor and a conjugated polymer (or small molecule) as the electron donor.[5–7] Among the high-performing polymer donors, diketopyrrolopyrrole (DPP) building block is considered as one of the most promising structural motif because of its strong electron-withdrawing property and large π-conjugated backbone along with relatively easy functionalization on the nitrogen atom of the pyrrole unit.[8–12] In fact, when copolymerized with electron-donating building blocks to form an electron push-pull material, DPP-based polymers feature a broad absorption range and a low band gap (E_g).[13,14] These characteristics are beneficial for high light-harvesting capability, in some cases extending absorption up to 1000 nm,[15,16] and improving transport properties, leading to high short-circuit current densities (J_{sc}) exceeding 20 mA cm^{-2} and mobilities over 12 cm^2 $V^{-1}s^{-1}$.[17–20] However, one of the main limitation that hinders the power conversion efficiency (PCE) of DPP-based OSCs is the relatively low open-circuit voltage (V_{oc}), which can be ascribed to high-lying ionization potential (IP) (*vs.* vacuum) of DPP derivatives as well as the fixed electron affinity (EA) of fullerenes derivatives.[21,22] To overcome this limitation, two simple energetic strategies can be considered: i) decrease the IP of the DPP donor or ii) increase the EA of the acceptor material. The first approach has been successfully investigated where a series of DPP-based polymers were designed with an introduction of a thiazole group (strong electronegativity nitrogen atoms in the building block), and thus, decreasing the IP level of the polymer (PDPP2Tz2T).[8] This strategy successively resulted high V_{oc} of 0.92 V OSCs with a low E_{loss} ($E_{loss} = E_g - qV_{oc}$) of 0.55 eV, where $PC_{71}BM$ was used as electron acceptor. However, the

devices were still limited by low J_{sc} and external quantum efficiency (EQE) below 40% due to the trade-off between voltage and photocurrent. On the other hand, recently emerged non-fullerene acceptors (NFAs) provide tunable optical bandgap as well as controllable crystallinity through molecular design, which is superior over fullerene derivatives. [7,23–26] Utilizing the tunable energetic levels (IP or EA) of NFAs, several acceptor molecules such as ITIC, SdiPBI small molecules and N2200 polymer were used in combination with DPP-thiophene based polymer donors for OSCs.[26–28] These devices, however, delivered low efficiencies (less than 5%) due to the limited fill factor (FF) and J_{sc}. Although the blend of NFA materials with commonly known donor molecules such as PTB7-Th and PBDB-T achieved up to 14% single junction solar cells, high quantum efficiency NFA-OSCs with decent photo-voltages using commercially viable and stable DPP polymers does not yet exist in literature.

Herein, we show for the first time highly efficient DPP:NFA BHJ solar cells with power conversion efficiency (PCE) of 8.14%, where PBDTT-DPP polymer donor is blended with the low bandgap IEICO-4F nonfullerene acceptor molecule (1.24 eV) (**Figure 1a**). PBDTT-DPP (DPP- benzodithiophene with alkylthiophene substituted groups (BDTT)) was selected as donor material for two reasons: i) BDTT block features a stronger intermolecular π-π interaction than thiophene units by extending the conjugation in the backbone and thus, facilitates better charge transport; and ii) BDTT is a weak electron-donating unit as compared to the thiophene units, which is a potential strategy to increase the V_{oc} with lowering the IP level of donor. Indeed, PBDTT-DPP:IEICO-4F devices obtained a PCE of 8.14% with a J_{sc} of 18.5 mA cm^{-2} and V_{oc} of 0.68 V with a small E_{loss} of 0.57 eV. We investigate the origin of the efficient devices in terms of optoelectronic measurements and nanomorphology, and compare the photovoltaic performance and electronic properties of devices fabricated with ITIC analogues (one of most commonly used state-of-the-art NFA) (**Figure 1a**).[29] In fact, we observe that the molecular properties of NFAs have strong influence on molecular ordering,

charge generation, transport and recombination in combination with DPP donor-based blends. As a result, due to the stronger intramolecular effect and crystallinity of IEICO-4F than that of ITIC, the corresponding devices possess efficient charge generation and low charge recombination compared to ITIC based devices. More interestingly, we used a combination of PEDOT:PSS:WOx and aluminium doped zinc oxide (AZO) nanoparticle/Phen-NaDPO bilayer as hole-transporting and electron- transporting layer, respectively, to promote charge extraction. Indeed, PBDTT-DPP:IEICO-4F BHJ delivered a PCE of 9.68%, which among the best for DPP polymers.

2. Results and Discussion

The thin-film ultraviolet-visible (UV-Vis) absorbance spectra of PBDTT-DPP, ITIC, and IEICO-4F are shown in **Figure 1b**, where the absorbance onset of IEICO-4F (E_g:1.24 eV) is 200 nm redshifted than that of ITIC (absorption onset of 800 nm).[30] In addition, as shown in **Figure S1,** whereas the absorption range of PBDTT-DPP:ITIC blend is limited to ca. 850 nm, PBDTT-DPP:IEICO-4F blend film features a broad absorption range (from 300 nm to 1000 nm), suggesting a better match with the solar spectrum. To compare these NFA based devices on their respective device performances, we fabricated the PBDTT-DPP based OSC devices and test under the AM 1.5 G illumination at 100 mW cm^{-2}. Device fabrication conditions, such as device structure, D:A weight ratio, solvent additives and active layer thickness, are varied to obtain the optimized conditions (**Figure S2-S6** and **Table S1-S5**). The best devices are constructed in a conventional configuration based on ITO/PEDOT:PSS(~40 nm)/Active layer (~100 nm)/Ca(~10 nm)/Al (~100 nm). The active layer consist of a 1:1.5 weight ratio of donor:acceptor (D:A) dissolved in a 99:1 v/v chlorobenzene (CB) with:1-chloronaphthalene (CN) solution. The summary of champion photovoltaic parameters and the corresponding *J-V* curves of PBDTT-DPP:ITIC and PBDTT-DPP:IEICO-4F are depicted in **Figure 2a** and summarized in **Table 1**. The optimized IEICO-4F based device yields a J_{sc} = 18.5 mA cm^{-2} V_{oc} = 679 mV and FF = 64.8%. In contrast, the ITIC-based device shows a J_{sc}

of 7.4 mA cm^{-2}, V_{oc} of 844 mV and FF of 59.2 %, yielding a PCE of 3.70%. As a comparison, we also fabricated PBDTT-DPP:$PC_{71}BM$ based devices, and, similar to previously reported results,[29] we obtained PCE of 6.97% (**Figure S7a**). The external quantum efficiency (EQE) spectra of corresponding devices are presented in **Figure 2b**. The integrated current density values extracted from EQE spectra matches well with the data from the *J-V* curves (with a mismatch less than 5%). In particular, IEICO-4F based device shows a higher and broader EQE (with the maximum value of 70% at 830 nm) from 300 nm to 1000 nm, significantly outperforming the one extracted from ITIC devices (EQE less than 30%) and $PC_{71}BM$ devices (lower than 60%, **Figure S7b**).

As discussed above, another critical parameter for DPP based devices is E_{loss}. In our case, fluorination in terminal block in the IEICO-4F results in a narrower bandgap and lower-lying EA level, which reduces the V_{oc} compared to the ITIC-based solar cells.[31] On the other hand, benefiting from the low optical bandgap and better spectral match of IEICO-4F, PBDTT-DPP:IEICO-4F devices exhibits a lower E_{loss} ca. 0.57 eV, calculated from the band edge from EQE (at 1.24 eV), whereas the E_{loss} for ITIC devices is 0.61 eV (considering to the lower bandgap of PBDTT-DPP, 1.46 eV). For comparison, the E_{loss} is 0.70 eV for the $PC_{71}BM$-based OSCs, demonstrating not only the superiority of IEICO-4F over ITIC but also the significant advantage of mixing low bandgap NFAs with PBDTT-DPP over fullerene derivatives.[4,32] We further demonstrate the advantage of IEICO-4F by compiling a number of previously reported results on the DPP based solar cells with both the $PC_{71}BM$ and different NFAs in **Figure 2c.** Here, EQE_{max} *vs.* E_{loss} are plotted from the literature ($PC_{71}BM$ devices, black squares and different NFA-based devices, red circles) along with the finding of this study of PBDTT-DPP:IEICO-4F (blue triangle), showing the smallest E_{loss} with the highest EQE_{max}.

To elucidate the smaller E_{loss} in IEICO-4F devices, Fourier transform photocurrent spectroscopy (FTPS) measurement has been carried out on both devices (**Figure S8**). IEICO-

4F based devices feature a sharper optical edge compared to ITIC solar cells. The reason for this feature could lie in the charge transfer state characteristics lowering non-radiative losses in PBDTT-DPP:IEICO-4F.[32–35]

We proceed to understand the photo-physics of these two devices. **Figure 3a** shows the charge generation and collection efficiencies by plotting the photocurrent density (J_{ph}) as a function of effective voltage (V_{eff}) under the illumination at 100 mW cm^{-2}. J_{ph} is equal to $J_l - J_d$, where J_l and J_d are the current density under illumination at 100 mW cm^{-2} and in the dark, respectively. V_{eff} is equal to $V_0 - V$; V_0 is the compensation voltage defined J_{ph} (V_0) = 0, and V is the applied voltage.[35] As illustrated in **Figure 3a** with the J_{ph} - V_{eff} plots, J_{ph} quickly saturates when V_{eff} is below 1 V in the case of IEICO-4F devices, whereas ITIC devices present a strong dependence of J_{ph} with V_{eff}, suggesting that generated electron-hole pairs are not efficiently dissociated and collected at the electrodes. In saturation condition, the maximum generation rate of free carriers, $G_{max,}$ is calculated according to $J_{sat} = qG_{max}L$, where q is the electron charge and L is the photoactive layer thickness. Following this equation, the G_{max} values obtained for IEICO-4F and ITIC -based devices are 9.25× 10^{21} and 6.04 × 10^{21} cm^{-3} s^{-1}, respectively, in line with the higher J_{sc} delivered in PBDTT-DPP:IEICO-4F devices. Moreover, we extract G values in the maximum power point G_{mpp} (MPP: maximum power point of J-V curves) and under short-circuit conditions G_{sc} (V=0). In details, the G_{sc} values for ITIC and IEICO-4F devices are 64% and 81% of G_{max}, respectively, while the G_{mpp} values for ITIC and IEICO-4F devices are 41% and 68% of G_{max}, respectively. The substantial difference in G values demonstrates the limitation of charge dissociation and extraction, and thus, lower J_{sc} and FF in the ITIC devices.

We further focus on the recombination mechanisms to fully understand the improved FF of IEICO-4F-based devices. By plotting J-V curves as a function of illumination intensity, a power-law dependence of J_{sc} on light intensity (P) was observed and was described as $J_{sc} \propto P_{in}^{S}$, ($P_{in}$ is the light intensity and s is the power law exponent), whereby s = 1 suggests

that all dissociated carriers are swept-out before the recombination process takes place, while s < 1 implies a bimolecular recombination (*i.e.* some carriers are recombined during the extraction process).[5,36] As shown in **Figure 3b**, the slopes (*s*) fitted from J_{sc} *vs* light intensity plots are 0.85 and 0.99 for PBDTT-DPP:ITIC and PBDTT-DPP:IEICO-4F devices, respectively; this points to higher bimolecular recombination in ITIC devices, whereas IEICO-4F does not show limitation on the bimolecular recombination. Then, we turn our attention into the trap-assisted recombination, which can be observed with the dependence of the open-circuit voltage *vs.* the light intensity.[37] Generally, a slope of *kT/q* (where *k* is defined as Boltzmann's constant, *T* is the Kelvin temperature and *q* is the elementary charge) in the plot of V_{oc} *vs* the natural logarithm of the light intensity is expected as pure bimolecular recombination (*i.e.* absence of trap assisted recombination), whereas a slope of 2*kT/q* implies that the trap-assisted recombination is a significant channel for carrier recombination. As depicted in **Figure 3c**, the slopes of 1.36 *kT/q* and 1.13 *kT/q* are obtained for PBDTT-DPP:ITIC and PBDTT-DPP:IEICO-4F devices, respectively; this demonstrates that the trap-assisted recombination is weaker in IEICO-4F devices, whereas ITIC-based devices are limited by trap formation.

In light of the V_{oc} *vs* light intensity measurements, we employ transient photo-voltage (TPV) method to better understand the recombination process, especially the carrier lifetimes (τ) (at open-circuit condition),[38,39] as shown in **Figure 3d**. The carrier lifetimes of the devices were extracted from the exponential fitting on the decay of the transient photo-voltage. As depicted in **Figure 3d**, ITIC based devices exhibited a longer lifetime (17.3 μs) due to a trap-released process.[36] Differently, IEICO-4F based devices exhibit a lifetime twice as short (7.7 μs) than that of ITIC. This results are in agreement with the higher trap assisted recombination observed in the plot of V_{oc} *vs* light intensity, which further confirmed the relatively lower FF values in ITIC devices.[40] Besides charge recombination, charge transport

is another crucial process for efficient organic photovoltaics. For this purpose, we measured the carrier mobility (μ) by employing the technique of photo-induced charge carrier extraction by linearly increasing voltage (Photo-CELIV) (**Figure S9)**. [41] The higher carrier mobility (μ) of IEICO-4F device (7.21×10^{-4} $cm^2\ V^{-1}\ s^{-1}$) indicates a better charge transport than that of ITIC-based devices (5.32×10^{-4} $cm^2\ V^{-1}\ s^{-1}$), which is consistent with higher FF observed in IEICO-4F devices.

The photo-physics of BHJ OSC are often associated with the blend microstructure. For this reason, we studied molecular orientation of the donor and acceptor materials at nanoscale by using grazing incidence wide-angle X-ray scattering (GIWAXS) [7], see **Figure 4.**Along with the 2D GIWAXS patterns of two neat NFA materials (**Figure 4a,b**), blend films with PBDTT-DPP (**Figure 4c,d**), and their corresponding sector averaged (± 7.5º) profiles in the In Plane (IP) and Out Of Plane (OOP) directions are shown (**Figure 4e)**. Firstly, the neat ITIC acceptor film (**Figure 4a** and **S11**), presents only a broad lamella stacking diffraction arc with an indistinct π- π stacking signature exhibiting a d-spacing ~ 4.1 Å. In contrast, with higher order lamellar stacking peaks both in the OOP and IP directions, IEICO-4F exhibits (**Figure 4b** and **S12**) an intense π- π stacking peak in the OOP direction with a shorter d-spacing ~ 3.7 Å, illustrating a typical face-on molecular orientation. . This findings corroborates to the previous reports, where fluorination increased the intermolecular interaction in BHJ blends.[43] Finally, we investigate the blend films (**Figure 4c** and **4d**), and observe that both the blends still remain largely face-on with π- π stacking peak in the OOP direction. Interestingly however, similar to their neat counterparts, differences in the π- π stacking peak are also evident between these two blends. As can be seen in the sector averaged (± 7.5 º) OOP profile in **Figure 4e**, IEICO-4F blend (blue solid line) exhibits a sharp π- π stacking peak with smaller full width half maximum compared to a broad and indistinct peak in the ITIC blend (red solid line). As a result, the d-spacing calculated from these peaks is found to be higher in the IEICO-4F blend (~ 3.3 Å) than ITIC counterparts (~ 3.7 Å). Taken altogether,

GIWAXS reveals better texture and molecular packing in the IEICO-4F blends which likely contributes to the charge transport, and thus, to its superior device performance as compared to the ITIC based devices.[11]

Finally, to gain further insights into the nanomorphology of PBDTT-DPP:NFA blends, and to make a comparison with fullerene based counterparts, transmission electron microscopy (TEM) and atomic force microscopy (AFM) characterizations were employed.[44–46] In earlier reports, DPP based polymers show a substantial molecular self-aggregation (strong intermolecular interaction), which would easily induce the "nanofiber" blend networks in DPP polymer:fullerene blends.[47] As shown in **Figure S13a** and **b**, IEICO-4F-based blend film exhibits a homogenous intermixed morphology in TEM images, while ITIC-based films displays relatively dispersed domains.[48] AFM images (**Figure S13c** and **d**) show that the PBDTT-DPP:IEICO-4F blend features a smooth surface, whereas the ITIC based film exhibits a rougher surface with root-mean square (RMS) exceeding 5 nm.

To further evaluate the potential of our PBDTT-DPP:IEICO-4F devices, we modified the HTL and ETL by using a hybrid organic material and inorganic metal oxide, respectively. This strategy has been reported recently by Zhou et al. for improving the charge extraction capability of the interfacial layers. [49] Fig. 5a and 5b depict the J-V characteristics and EQE curves for the resulting ternary devices with the modified HTL and ETL. As illustrated from Figure 5a and Table 2, the FF is improved from 64.8% to 68.2% after the WO_x incorporation into PEDOT:PSS at 1:1 volume ratio. Moreover, the superior charge extraction of this hybrid HTL is reflected in the enhanced EQE in the 400-600 nm spectral region compared to PEDOT-based devices. Furthermore, the high conductivity AZO nanoparticles were spin-coated on top of active layer, then a thin organic Phen-NaDPO layer was casted on the AZO layer, which is reported as an efficient strategy for both charge transport and charge collection.[50] Interestingly, all photovoltaic parameters show the subtle enhancement with the

hybrid AZO/ Phen-NaDPO ETL modification, delivering a champion PCE of 9.68% for PBDTT-DPP:IEICO-4F solar cells, which is one of the highest for DPP-based solar cells.

3. Conclusion

In conclusion, by combining a low-lying ionization potential DPP polymer (PBDTT-DPP) and IEICO-4F as electron-acceptor, we obtain organic solar cells delivering a power conversion efficiency (PCE) of 8.14%. When compared with ITIC blend, an optimal blend morphology with stronger molecular packing, enhanced charge generation and suppressed recombination allows efficient charge transport in the PBDTT-DPP:IEICO-4F based devices, resulting in a simultaneous improvement of J_{sc} and FF (J_{sc} = 18.5 mA cm^{-2}, V_{oc} = 679 mV and FF = 64.8%). Moreover, a relative low E_{loss} of 0.57 eV along with high EQE_{max} (>70%) for DPP:IEICO-4F devices are reported for the first time for this class of polymer in combination with NFA. Additionally, by using a hybrid HTL and ETL further boost the efficiency to 9.68%, which is among the highest PCE of DPP-based solar cells. Our work highlights that the intrinsic absorption strength and crystallinity of IEICO-4F is crucial to achieve high PCE in DPP solar cells. Furthermore, our results demonstrate the potential of high efficiency DPP polymer donor:non-fullerene acceptor OSC devices, and provide guideline for future molecular design of non-fullerene acceptors for DPP-based polymer donors.

Supporting Information ((delete if not applicable))
Supporting Information is available from the Wiley Online Library or from the author.

1. Acknowledgements

D. Baran acknowledges KAUST Solar Center Competitive Fund (CCF) for financial support. Prof. W. Li thanks the financial support from NSFC (21574138 and 91633301). GIWAXS measurement and analysis, done by M. M. Nahid and H. Ade, are supported by ONR grant N000141712204 and KAUST's Center Partnership Fund (No. 3321). X-ray data were acquired at beamlines 7.3.3 at the Advanced Light Source (ALS) in Berkeley National Lab, which is supported by the U.S. Department of Energy (DE-AC02-05CH11231). Z. Peng, S.

Stuard, and I. Angunawela assisted with the GIWAXS data acquisition. C. Zhu is acknowledged for the beamline support.

Received: ((will be filled in by the editorial staff))
Revised: ((will be filled in by the editorial staff))
Published online: ((will be filled in by the editorial staff))

References

[1] Y. J. Cheng, S. H. Yang, C. S. Hsu, *Chem. Rev.* **2009**, *109*, 5868.

[2] J. Zhao, Y. Li, G. Yang, K. Jiang, H. Lin, H. Ade, W. Ma, H. Yan, Efficient organic solar cells processed from hydrocarbon solvents. *Nat. Energy* **2016**, *1*, 15027.

[3] B. Fan, L. Ying, P. Zhu, F. Pan, F. Liu, J. Chen, F. Huang, Y. Cao, All-Polymer Solar Cells Based on a Conjugated Polymer Containing Siloxane-Functionalized Side Chains with Efficiency over 10%. *Adv. Mater.* **2017**, *29*, 1703906.

[4] J. Hou, O. Inganäs, R. H. Friend, F. Gao, *Nat. Mater.* **2018**, *17*, 119.

[5] X. Song, N. Gasparini, D. Baran, *Adv. Electron. Mater.* **2017**, *2*, 1700358.

[6] Y. Liu, J. Zhao, Z. Li, C. Mu, W. Ma, H. Hu, K. Jiang, H. Lin, H. Ade, H. Yan, *Nat. Commun.* **2014**, *5*, 5293.

[7] X. Song, N. Gasparini, M. M. Nahid, H. Chen, S. M. Macphee, W. Zhang, V. Norman, C. Zhu, D. Bryant, H. Ade, I. McCulloch, D. Baran, *Adv. Funct. Mater.* **2018**, *30*, 1802895.

[8] W. Li, K. H. Hendriks, A. Furlan, M. M. Wienk, R. A. J. Janssen, *J. Am. Chem. Soc.* **2015**, *137*, 2231.

[9] W. Li, K. H. Hendriks, A. Furlan, W. S. C. Roelofs, M. M. Wienk, R. A. J. Janssen, *J. Am. Chem. Soc.* **2013**, *135*, 18942.

[10] L. Lu, T. Zheng, Q. Wu, A. M. Schneider, D. Zhao, L. Yu, *Chem. Rev.* **2015**, *115*, 12666.

[11] C. Huang, X. Liao, K. Gao, L. Zuo, F. Lin, X. Shi, C.-Z. Li, H. Liu, X. Li, F. Liu, Y.

Chen, H. Chen, A. K.-Y. Jen, *Chem. Mater.* **2018**, *30*, 5429.

[12] J. Sun, X. Ma, Z. Zhang, J. Yu, J. Zhou, X. Yin, L. Yang, R. Geng, R. Zhu, F. Zhang, W. Tang, *Adv. Mater.* **2018**, *30*, 1707150.

[13] W. Li, K. H. Hendriks, M. M. Wienk, R. A. J. Janssen, *Acc. Chem. Res.* **2016**, *49*, 78.

[14] W. Li, K. H. Hendriks, W. S. C. Roelofs, Y. Kim, M. M. Wienk, R. A. J. Janssen, *Adv. Mater.* **2013**, *25*, 3182.

[15] G. Oklem, X. Song, L. Toppare, D. Baran, G. Gunbas, *J. Mater. Chem. C* **2018**, *6*, 2957.

[16] E. Zhou, K. Hashimoto, K. Tajima, *Polym. (United Kingdom)* **2013**, *54*, 6501.

[17] H. Choi, S.-J. Ko, T. Kim, P.-O. Morin, B. Walker, B. H. Lee, M. Leclerc, J. Y. Kim, A. J. Heeger, *Adv. Mater.* **2015**, *27*, 3318.

[18] W. Shockley, H. J. Queisser, *J. Appl. Phys.* **1961**, *32*, 510.

[19] C. B. Nielsen, M. Turbiez, I. McCulloch, *Adv. Mater.* **2013**, *25*, 1859.

[20] Y. Ji, C. Xiao, Q. Wang, J. Zhang, C. Li, Y. Wu, Z. Wei, X. Zhan, W. Hu, Z. Wang, R. A. J. Janssen, W. Li, *Adv. Mater.* **2016**, *28*, 943.

[21] W. Li, K. H. Hendriks, M. M. Wienk, R. A. J. Janssen, Acc. Chem. Res., **2015**, *49*, 78.

[22] M. Li, J. Li, D. Di Carlo Rasi, F. J. M. Colberts, J. Wang, G. H. L. Heintges, B. Lin, W. Li, W. Ma, M. M. Wienk, R. A. J. Janssen, *Adv. Energy Mater.* **2018**, *8*, 1800550.

[23] N. Gasparini, A. Wadsworth, M. Moser, D. Baran, I. Mcculloch, C. J. Brabec, *Adv. Energy Mater.* **2018**, *8*, 1703298.

[24] X. Liu, X. Li, Y. Li, C. Song, L. Zhu, W. Zhang, H.-Q. Wang, J. Fang, *Adv. Mater*. **2016**, *28*, 7405.

[25] S. Liu, X. Song, S. Thomas, Z. Kan, F. Cruciani, F. Laquai, J.-L. Bredas, P. M. Beaujuge, *Adv. Energy Mater.* **2017**, *7*, 1602574.

[26] C. Li, A. Zhang, Z. Wang, F. Liu, Y. Zhou, T. P. Russell, Y. Li, W. Li, *RSC Adv.* **2016**, *6*, 35677.

[27] X. Jiang, Y. Xu, X. Wang, Y. Wu, G. Feng, C. Li, W. Ma, W. Li, *Phys. Chem. Chem. Phys.* **2017**, *19*, 8069.

[28] C. Li, A. Zhang, G. Feng, F. Yang, X. Jiang, Y. Yu, D. Xia, W. Li, *Org. Electron. physics, Mater. Appl.* **2016**, *35*, 112.

[29] L. Dou, J. You, J. Yang, C. C. Chen, Y. He, S. Murase, T. Moriarty, K. Emery, G. Li, Y. Yang, *Nat. Photonics* **2012**, *6*, 180.

[30] Y. (Michael) Yang, W. Chen, L. Dou, W.-H. Chang, H.-S. Duan, B. Bob, G. Li, Y. Yang, *Nat. Photonics* **2015**, *9*, 190.

[31] S. Li, L. Ye, W. Zhao, S. Zhang, H. Ade, J. Hou,. *Adv. Energy Mater.* **2017**, *7*, 1700183.

[32] D. Baran, T. Kirchartz, S. Wheeler, S. Dimitrov, M. Abdelsamie, J. Gorman, R. S. Ashraf, S. Holliday, A. Wadsworth, N. Gasparini, P. Kaienburg, H. Yan, A. Amassian, C. J. Brabec, J. R. Durrant, I. McCulloch, *Energy Environ. Sci.* **2016**, *9*, 3783.

[33] H. Fu, Y. Wang, D. Meng, Z. Ma, Y. Li, F. Gao, Z. Wang, Y. Sun, *ACS Energy Lett.* **2018**, *3*, 2729.

[34] J. Liu, S. Chen, D. Qian, B. Gautam, G. Yang, J. Zhao, J. Bergqvist, F. Zhang, W. Ma, H. Ade, O. Inganäs, K. Gundogdu, F. Gao, H. Yan, Fast charge separation in a non-fullerene organic solar cell with a small driving force. *Nature Energy*. **2016**, *1*, 16089.

[35] N. Gasparini, M. Salvador, S. Strohm, T. Heumueller, I. Levchuk, A. Wadsworth, J. H. Bannock, J. C. de Mello, H.-J. Egelhaaf, D. Baran, I. McCulloch, C. J. Brabec, *Adv. Energy Mater.* **2017**, *7*, 1700770.

[36] X. Song, N. Gasparini, L. Ye, H. Yao, J. Hou, H. Ade, D. Baran, *ACS Energy Lett.* **2018**, *3*, 669.

[37] W. L. Leong, S. R. Cowan, A. J. Heeger, *Adv. Energy Mater.* **2011**, *1*, 517.

[38] D. Baran, R. S. Ashraf, D. A. Hanifi, M. Abdelsamie, N. Gasparini, J. A. Röhr, S. Holliday, A. Wadsworth, S. Lockett, M. Neophytou, C. J. M. Emmott, J. Nelson, C. J.

Brabec, A. Amassian, A. Salleo, T. Kirchartz, J. R. Durrant, I. McCulloch, *Nat. Mater.* **2017**, *16*, 363.

[39] S. Holliday, R. S. Ashraf, A. Wadsworth, D. Baran, S. A. Yousaf, C. B. Nielsen, C.-H. Tan, S. D. Dimitrov, Z. Shang, N. Gasparini, M. Alamoudi, F. Laquai, C. J. Brabec, A. Salleo, J. R. Durrant, I. McCulloch, *Nat. Commun.* **2016**, *7*, 11585.

[40] N. A. Ran, J. A. Love, M. C. Heiber, X. Jiao, M. P. Hughes, A. Karki, M. Wang, V. V. Brus, H. Wang, D. Neher, H. Ade, G. C. Bazan, T.-Q. Nguyen, Charge Generation and Recombination in an Organic Solar Cell with Low Energetic Offsets. *Adv. Energy Mater.* **2017**, *7*, 1701073.

[41] N. Gasparini, X. Jiao, T. Heumueller, D. Baran, G. J. Matt, S. Fladischer, E. Spiecker, H. Ade, C. J. Brabec, T. Ameri, *Nat. Energy* **2016**, *1*, 16118.

[42] J. R. Tumbleston, B. A. Collins, L. Yang, A. C. Stuart, E. Gann, W. Ma, W. You, H. Ade, *Nat. Photonics* **2014**, *8*, 385.

[43] S. Dai, F. Zhao, Q. Zhang, T.-K. Lau, T. Li, K. Liu, Q. Ling, C. Wang, X. Lu, W. You, X. Zhan, *J. Am. Chem. Soc.* **2017**, *139*, 1336.

[44] L. Ye, H. Hu, M. Ghasemi, T. Wang, B. A. Collins, J.-H. Kim, K. Jiang, J. H. Carpenter, H. Li, Z. Li, T. McAfee, J. Zhao, X. Chen, J. L. Y. Lai, T. Ma, J.-L. Bredas, H. Yan, H. Ade, *Nat. Mater.* **2018**, *17*, 253.

[45] X. Jiao, L. Ye, H. Ade, *Adv. Energy Mater.* **2017**, *7*, 1700084.

[46] E. Gann, B. A. Collins, M. Tang, J. R. Tumbleston, S. Mukherjee, H. Ade, *J. Synchrotron Radiat.* **2016**, *23*, 219.

[47] W. Li, K. H. Hendriks, A. Furlan, W. S. C. Roelofs, S. C. J. Meskers, M. M. Wienk, R. A. J. Janssen, *Adv. Mater.* **2014**, *26*, 1565.

[48] W. Li, L. Ye, S. Li, H. Yao, H. Ade, J. Hou, *Adv. Mater.* **2018**, *30*, 1707170.

[49] Z. Zheng, Q. Hu, S. Zhang, D. Zhang, J. Wang, S. Xie, R. Wang, Y. Qin, W. Li, L. Hong, N. Liang, F. Liu, Y. Zhang, Z. Wei, Z. Tang, T. P. Russell, J. Hou, H. Zhou, *Adv.*

Mater. **2018**, *30*, 1801801.

[50] X. Song, N. Gasparini, M. M. Nahid, S. H. K. Paleti, J.-L. Wang, H. Ade, D. Baran, *Joule* **2019**, DOI:10.1016/j.joule.2019.01.009.

Figures :

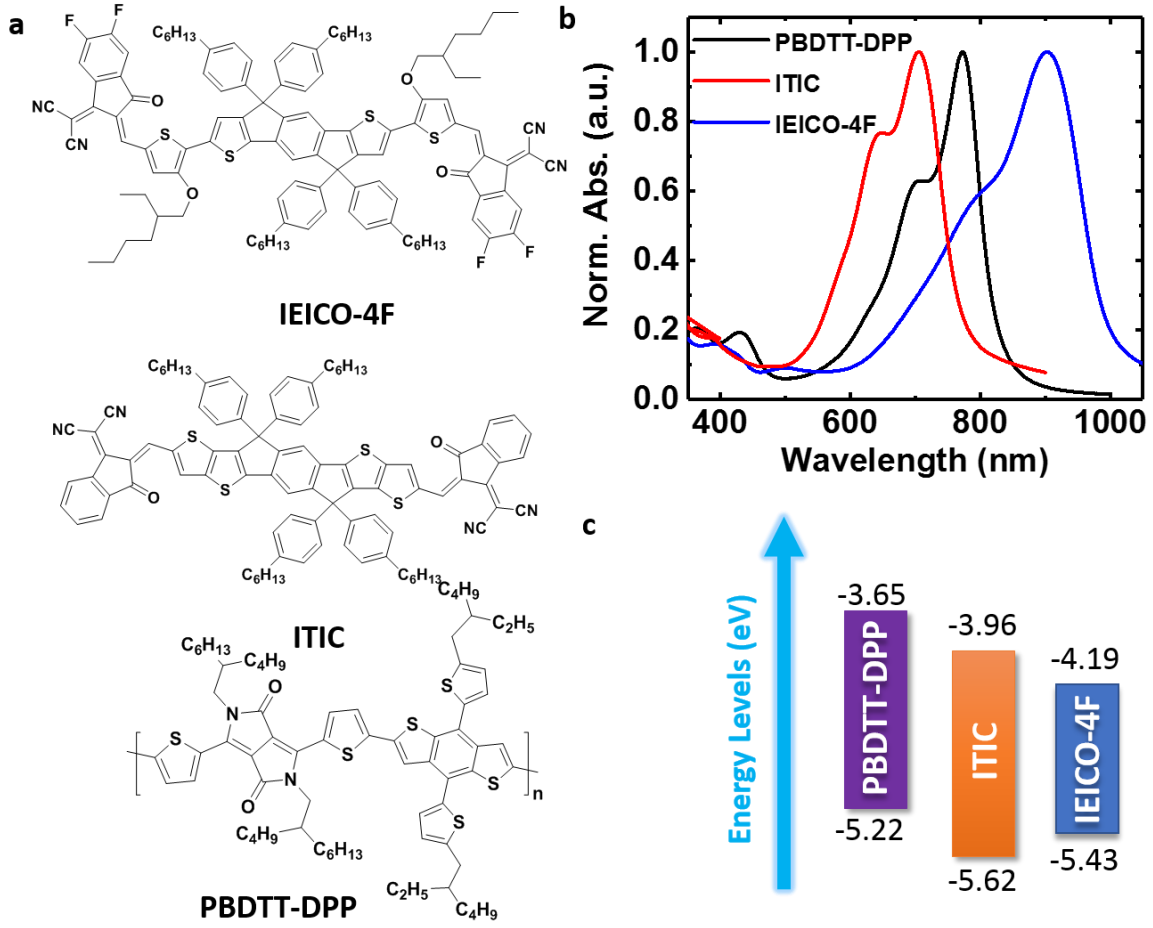

Figure 1: a) The molecular structure; b) normalized absorbance spectra (neat films) and c) energy level diagram of donor PBDTT-DPP and acceptors IEICO-4F and ITIC.

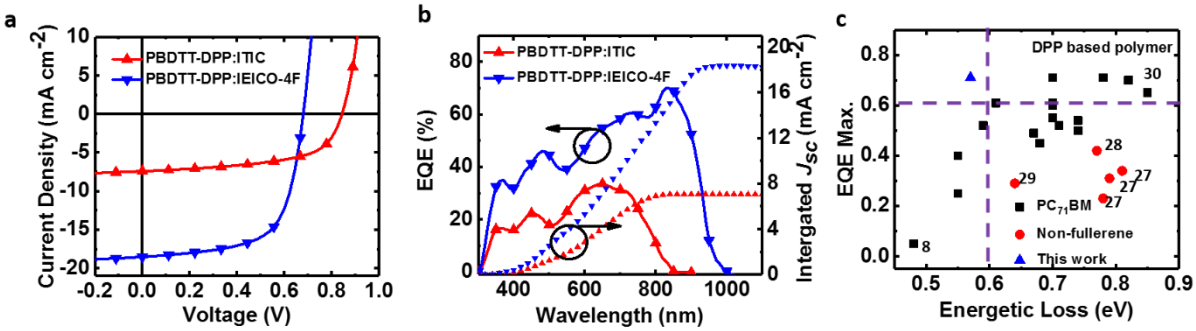

Figure 2: a) J-V curves, and b) EQE curves with integrated J_{sc} of the PBDTT-DPP:ITIC and PBDTT-DPP:IEICO-4F devices. c) EQE_{max} *versus* E_{loss} plot of the reported DPP based organic solar cells. The result from this study is shown in blue-triangle.

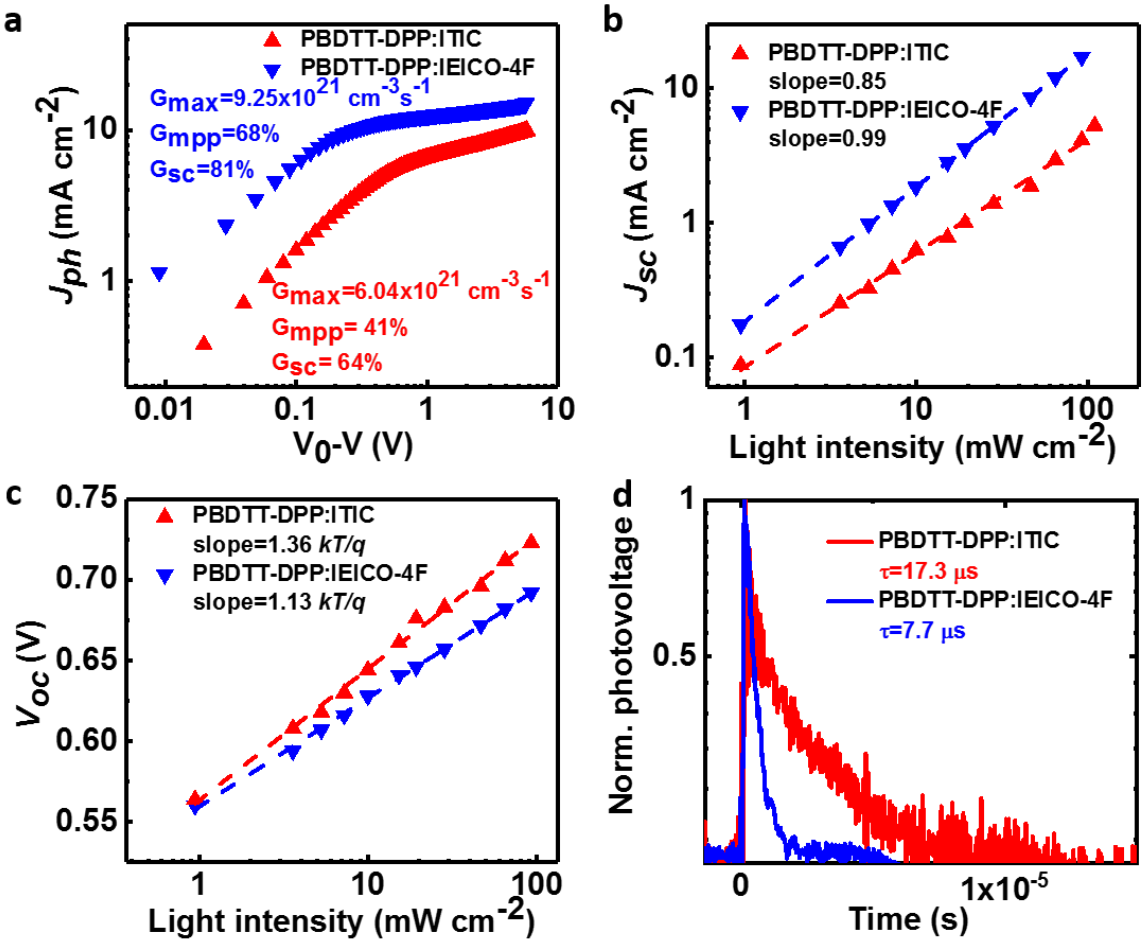

Figure 3: a): Photocurrent density as a function of the effective voltage at 100 mW/cm^2 illumination. Short-circuit current density (b) and open-circuit voltage (c) under different light intensities of PBDTT-DPP:ITIC and PBDTT-DPP:IEICO-4F devices. d) TPV plots of PBDTT-DPP:ITIC and PBDTT-DPP:IEICO-4F devices.

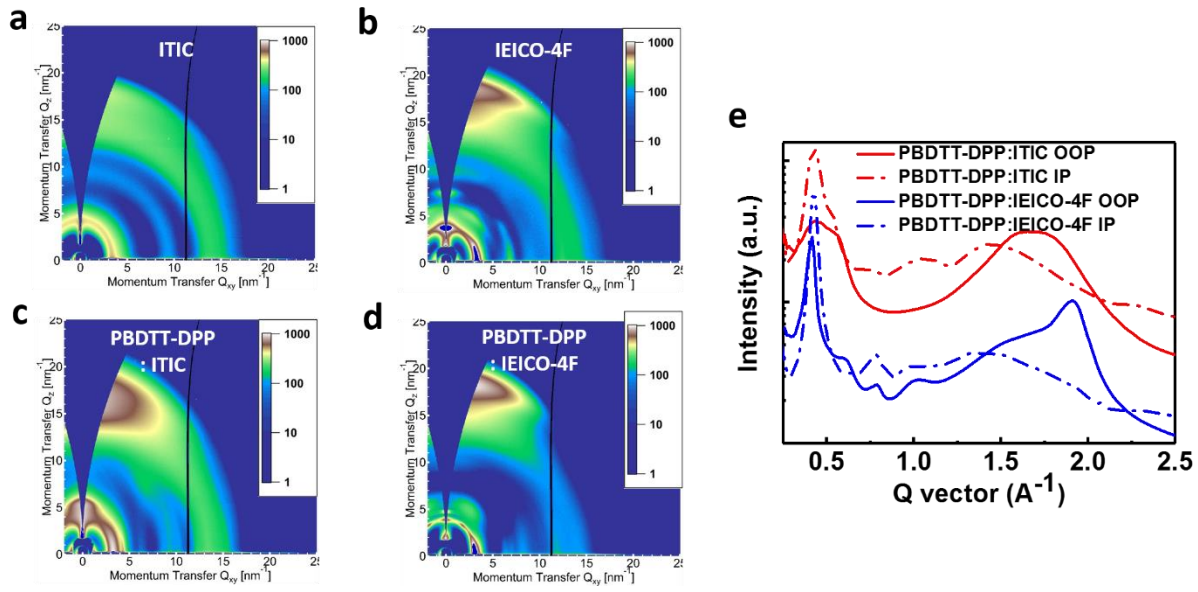

Figure 4. 2D GIWAXS patterns of (a) ITIC, (b) IEICO-4F, (c) PBDTT-DPP:ITIC and (d) PBDTT-DPP:IEICO-4F, and (e) 1D in-plane (IP) and Out OF Plane (OOP) sector profiles of the blends.

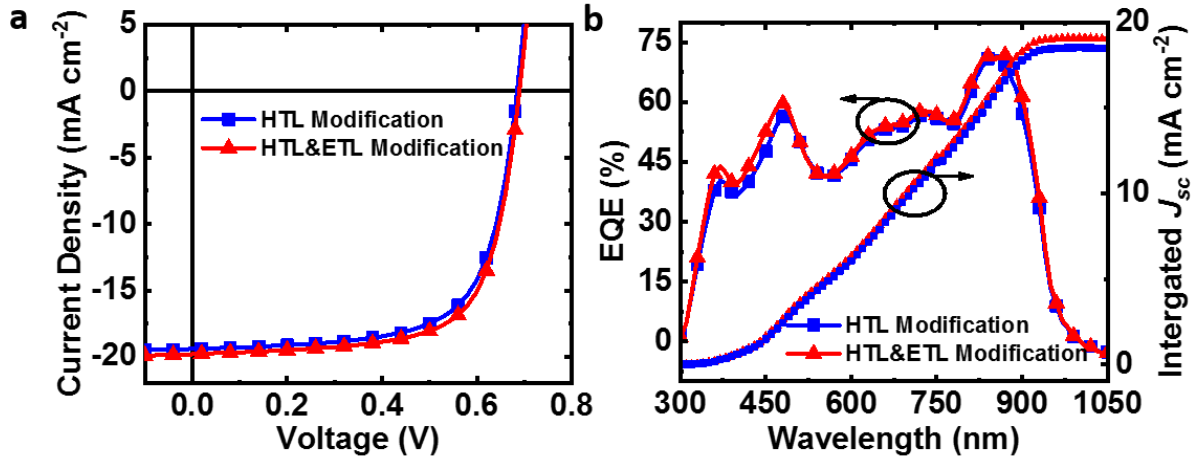

Figure 5. J–V characteristics (a) and spectrally resolved EQEs (b) of modified HTL and ETL interface layer of PBDTT-DPP:IEICO-4F system.

Table 1. Photovoltaic parameters of the PBDTT-DPP based OSCs blended with ITIC and PBDTT-DPP:IEICO-4F.

Blend Film	J_{sc} (mA/cm^2)	Integrated J_{sc} (mA/cm^2)	V_{oc} (mV)	FF (%)	PCE (%)	Ave PCE (%)[a]
PBDTT-DPP:ITIC	7.4	7.0	844	59.2	3.70	3.52
PBDTT-DPP:IEICO-4F	18.5	18.2	679	64.8	8.14	7.87

a : the average PCE values obtained from 10 devices.

Table 2. Photovoltaic parameters of the PBDTT-DPP:IEICO-4F devices with the modified HTL and ETL layer.

	J_{sc} (mA/cm^2)	Integrated J_{sc} (mA/cm^2)	V_{oc} (mV)	FF (%)	PCE (%)	Ave PCE (%)[a]
HTL	19.2	18.6	690	68.7	9.10	8.85
HTL&ETL	19.8	19.0	695	70.2	9.67	9.46

a : the average PCE values obtained from 10 devices.

The table of contents

Diketopyrrolopyrrole (DPP)-based polymers have gained a significant research interest in the organic electronics community. In this work, we use a combination of DPP polymer derivative, PBDTT-DPP, blending with IEICO-4F, a start-of-the-art small-molecule acceptor, yielding a champion power conversion efficiency (PCE) of 9.68%, among the best performance of DPP-based solar cells.

Keyword:
Diketopyrrolopyrrole, non-fullerene acceptor, low energetic loss, high quantum efficiency

Xin Song, Nicola Gasparini, Masrur Morshed Nahid, Sri Harish Kumar Paleti, Cheng Li, Weiwei Li, Harald Ade, Derya Baran*

Low energetic loss DPP donor and non-fullerene acceptor organic solar cells with high quantum efficiencies

ToC figure ((Please choose one size: 55 mm broad × 50 mm high **or** 110 mm broad × 20 mm high. Please do not use any other dimensions))

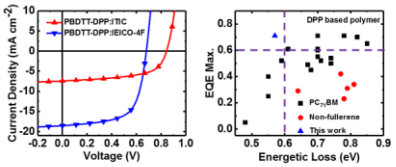

((Supporting Information can be included here using this template))

Supporting Information

Title ((no stars))

*Author(s), and Corresponding Author(s)** ((write out full first and last names))

((Please insert your Supporting Information text/figures here. Please note: Supporting Display items, should be referred to as Figure S1, Equation S2, etc., in the main text…)